Journal Pre-proof

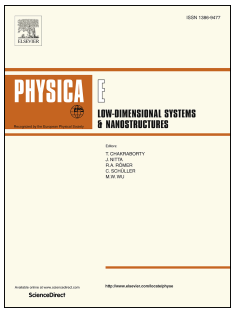

Strain Tunable Schottky Barriers and Tunneling Characteristics of Borophene/MX_2 van der Waals Heterostructures

Neha Katoch, Ashok Kumar, Raman Sharma, P.K. Ahluwalia, Jagdish Kumar

PII: S1386-9477(19)31256-1

DOI: https://doi.org/10.1016/j.physe.2019.113842

Reference: PHYSE 113842

To appear in: *Physica E: Low-dimensional Systems and Nanostructures*

Received Date: 19 August 2019

Revised Date: 29 October 2019

Accepted Date: 19 November 2019

Please cite this article as: N. Katoch, A. Kumar, R. Sharma, P.K. Ahluwalia, J. Kumar, Strain Tunable Schottky Barriers and Tunneling Characteristics of Borophene/MX_2 van der Waals Heterostructures, *Physica E: Low-dimensional Systems and Nanostructures* (2019), doi: https://doi.org/10.1016/j.physe.2019.113842.

Strain Tunable Schottky Barriers and Tunneling Characteristics of Borophene/MX_2 van der Waals Heterostructures

Neha Katoch[1*], Ashok Kumar[2], Raman Sharma[3], P.K. Ahluwalia[3] and Jagdish Kumar[1]

[1]*Department of Physics and Astronomical Science, School of Physical and Material Sciences, Central University of Himachal Pradesh, Dharamshala, 176215 (India)*

[2]*Department of Physical Science, School of Basic and Applied Sciences, Central University of Punjab, Bathinda, 151001(India)*

[3]*Department of Physics, Himachal Pradesh University, Shimla, 171005 (India)*

[*]Email:
Neha Katoch (nehakatoch2@gmail.com)

Abstract

In this paper, the strain induced changes in electronic properties and their influence on current-voltage ($I-V$) characteristics of the borophene (β_{12})/MX_2 (M = Mo, W and X = S, Se) vdW heterostructures are investigated within the framework of DFT. The results reveal that the intrinsic electronic nature of borophene and MX_2 is retained because of weak van der Waals interactions. However, p-type Schottky contacts are formed at the interface of the heterostructures. Application of the in-plane tensile and compression strains is effective in tuning the Schottky contacts and controlling the SBHs. Also at the vertical pressure values of 5.46 and 5.25 GPa for β_{12}/MoS_2 and β_{12}/WS_2 respectively, Schottky contact changes from p-type to n-type. The $I-V$ characteristics exhibit an ohmic behavior at low bias $\pm 0.1\ V$ and noticeable NDR, on changing positive (negative) biases. Such strain tunable Schottky barriers may be influential in β_{12}/MX_2 based high-performance nano- and optoelectronic devices.

1. Introduction

The interest in atomically thin two dimensional (2D) layered structures such as graphene, transition metal dichalcogenides (TMDs), boron nitride (BN), group-IV and group-V elements has increased in recent time because of their potential applications in the area of photonics, electronics, energy conversion and storage, and biomedical technologies with a possibility of replacing traditional materials [1-4]. Among 2D materials, TMDs are the most studied prospective layered structures on account of their novel properties such as band gap modulation by external perturbations [5,6], strong optoelectronic responses [7], outstanding carrier mobilities [8] and high structural flexibilities [9]. The study of 2D structures has also been extended to monoelemental group-III family due to the successful synthesis of borophene [10-12]. A unique blend of properties of borophene (β_{12}) such as lightest 2D metal [10], mechanically strong [13], optically transparent [14] and a promising anode material for batteries [15] makes it stand out as a distinctive technological material among 2D monoelemental structures.

It is well known that the properties of 2D materials can be tuned by constructing vertically-stacked van der Waals (vdW) heterostructures [2, 16] to realize electronic devices. Extensive studies have been carried out experimentally and theoretically for a wide range of vdW heterostructures, such as graphene/TMDs [17-21], graphene/h-BN [22], graphene/silicene [23], graphene/InSe [24], $MoTe_2/MoS_2$ [25], graphene/phosphorene and heterostructrues based on allotropes of phosphorene and $MoSe_2$ [26, 27]. These vdW heterostructures possess many advantageous properties due to interesting interface physics by integrating the isolated layers. Incorporating borophene having good metallic character with other 2D materials [28-30] has been expected to be a significant step in the design of new devices based on this kind of layered

structures. It is worth underlining the fact that junction formed at the contact between metallic and a semiconducting material is crucial in modern electronics and optoelectronics [31].

The Schottky barrier height (SBH) is an energy barrier for a charge carrier to cross the junction. It is a key parameter for the metal-semiconductor (MS) junction because the current flow across the MS interface depends on the magnitude of the SBHs. It determines the charge transport efficiency and can impact the device performance significantly [32]. It is previously shown that SBH can be reduced and ohmic contacts can be achieved in metal/semiconductor heterostructures by external electric field [26, 27], doping [32, 33] and mechanical strain [34, 35]. Ohmic contact formation at the heterointerface is generally advantageous for easy current flow between source/drain electrode and semiconductor [36], and good sensing performance which could be attributed to low charge transfer resistance [37]. Studies have also shown that the electronic properties and SBHs in graphene/MoS_2 can be controlled by changing the interlayer distance [38]. It is interesting to note that strain engineering is one of the best possible strategies for tuning the band gap of the 2D structures and is easy to realize experimentally as well [39, 40].

Strain dependent tuning of electronic properties as an important aspect needs to be explored systematically which we have chosen to do for borophene (β_{12})/MX_2 (M = Mo, W and X = S, Se) vdW heterostructures as an important class. Therefore, first-principles investigation of β_{12}/MX_2 heterostructures for tuning the Schottky barriers has been performed by applying in-plane uniaxial and biaxial strains (compression and expansion) and normal compression strains. In addition, the tunneling characteristics within Bardin, Tersoff and Hamman (BTH) formalism [41-43] have also been investigated for strained β_{12}/MX_2 heterostrcutures.

2. Computational Details

The calculations are carried out within the framework of density functional theory (DFT) as implemented in the Vienna ab-initio Simulation Package (VASP) [44]. The generalized gradient approximation (GGA), in Perdew, Burke, and Ernzerhof (PBE) parameterization [45] has been used to describe the exchange-correlation effects. The electron-ion interactions are taken into account using the Projector Augmented Wave (PAW) pseudopotential method [46]. The cutoff of plane-wave kinetic energy and the convergence criterion of energy in the self-consistency process have been set to be 700 eV and 10^{-6} eV, respectively. To describe the vdW interactions, vdW-D2 correction has been included in the present calculations [47]. A 15x9x1 k-point mesh has been employed for Brillouin zone integrations. The structural relaxations are performed to a force tolerance of 0.001 eV/Å by computing the Hellmann-Feynman forces using conjugate gradient algorithm. To minimize the lattice mismatch between the β_{12} and MX_2, the unit cell of the system is composed by 1x1 unit cell of β_{12} and 1x2 unit cells of MX_2 along X and Y directions. A vacuum region of more than 20 Å has been taken along the z-axis to remove the interactions between periodic images.

The effect of applying a normal in-plane uniaxial and biaxial compression (expansion) strains on the heterostructures is modelled by relaxing ion positions and calculating stress tensor keeping the cell shape constant. The modelling of an applied normal compression strain on the heterostructrues has been done by varying the interlayer distance, while keeping the atomic positions and the in-plane lattice vectors fixed so as to prevent relaxation of instantaneous structure to the original position. The full relaxation along the XY plane is expected not to change the in-plane lattice constants and electronic structure drastically [48].

3. Results and Discussion

There is no detectable geometric distortion shown by all of the studied MX_2 after contacting the monolayer of β_{12} as depicted by Figure 1. Note that lattice mismatch in β_{12}/MX_2 heterostructures is < 2% (Table 1). Binding energy (E_b) of heterostructure is calculated to be very small (Table 1) which shows given heterostructures to be vdW in nature. The binding energy E_b has been calculated as follows:

$$E_b = \left[E_{\beta 12 + MX_2} - E_{\beta 12} - E_{MoS_2}\right]/N \quad (1)$$

where $E_{\beta 12 + MX_2}$, $E_{\beta 12}$, E_{MX_2} and N are the total energy of β_{12}/MX_2 heterostructures, total energy of isolated β_{12} layer, total energy of isolated MX_2 layer and total number of atoms in the heterostructures, respectively.

TABLE 1. Calculated binding energies **(E_b)** per atom, interlayer distance **(d)** and average absolute interface surface lattice constant mismatch **(ε)** for pristine β_{12}/MX_2 heterostructures.

System	E_b (eV/atom)	d (Å)	ε (%)
β_{12}/MoS_2	-0.030	3.20	1.10
$\beta_{12}/MoSe_2$	-0.038	3.21	1.82
β_{12}/WS_2	-0.038	3.16	1.11
β_{12}/WSe_2	-0.044	3.20	1.11

3.1. Tensile Strength

In order to study the mechanical properties, it is worth investigating the strain-stress curves for β_{12}/MX_2 heterostructures under expansion strains. This curve can be obtained by calculating the constituents of stress tensor depending upon strain tensor. Stress tensor is defined as a positive derivative of total energy with respect to the strain tensor. In Figure 2 (a-d), the values of stress vary directly with the values of different strains up to some limit and then drop rapidly. This limit is known as the ideal strain strength of the system which is the potential of a system to tolerate load.

The values of ideal tensile strengths and ultimate strain for β_{12}/MX_2 heterostructures are listed in Table 2. The tensile strengths of the heterostructures follow the trend, β_{12}/MoS_2> β_{12}/WS_2 > $\beta_{12}/MoSe_2$ > β_{12}/WSe_2 which is implying that β_{12}/MoS_2 has the highest tensile strength and β_{12}/WSe_2 has the lowest tensile strength amongst the studied heterostructures under expansion strains (both uniaxial and biaxial).

TABLE 2. Calculated values of tensile strength (GPa) and ultimate tensile strains (%) for β_{12}/MX_2 heterostructures.

Systems	Tensile Strength (GPa)			Ultimate Strain (%)		
	+a	+b	+a+b	+a	+b	+a+b
β_{12}/MoS_2	3.96	3.72	6.12	20.0	12.5	10.5
$\beta_{12}/MoSe_2$	2.72	2.78	4.51	14.5	10.5	10.5
β_{12}/WS_2	3.89	3.29	5.99	20.0	14.0	10.5
β_{12}/WSe_2	2.66	2.69	4.40	15.0	10.5	8.50

3.2. Electronic Structure and Schottky Barriers

The orbital projected band structures (OPBS) of the β_{12}/MX_2 heterostructures show that the electronic nature of constituents monolayers remain preserved upon the heterostructure formation. OPBS reveal that the VBM and CBM are mainly associated with the d-orbitals of Mo and W of MX_2, whereas small contributions of S-p and Se-p orbital states are also found in CBM (Figure 3). From a device point of view, when metal (β_{12}) and semiconductor (MX_2) come in contact, there is electrical transport at MS interface and the states will be offset, thus, Fermi level is located below (or above) the midgap, known as the p-type (or n-type) Schottky barriers [30]. Therefore, Schottky barriers for holes $\emptyset_h$ or electrons $\emptyset_e$ are determined as the energy difference between the Fermi level (E_F) and the valence band maximum (VBM) or the conduction band minimum (CBM) of the heterostructures, respectively [31, 49] as shown in Figure 3(f). The SBHs for electrons and holes in considered heterostructures are listed in Table 3 which are consistent with the previous studies [50].

The trends in the SBHs can be attributed to the interlayer coupling in the formed vdW heterostructures which is also reflected by the charge density difference profiles as illustrated in Figure 3 (g-j). The charge density difference can be defined as:

$$\rho = \rho_{\beta 12 + MX_2} - \rho_{\beta 12} - \rho_{MX_2} \quad (2)$$

where $\rho_{\beta 12 + MX_2}$ represents the total charge density of the heterostructures, $\rho_{\beta 12}$ is the charge density of β_{12} and ρ_{MX_2} denotes the charge density of MX_2, respectively. The charge density difference plots provide the information about redistribution of electronic charges as a result of interlayer coupling due to heterostructure formation. Additionally, it can be seen from the plot of β_{12}/MoS_2 and β_{12}/WS_2, that small amount of charges is depleted on the β_{12} side and accumulated on MoS_2 and WS_2 side while in case of $\beta_{12}/MoSe_2$ and β_{12}/WSe_2, the accumulation of charges takes place near the β_{12} and depletion near the $MoSe_2$ and WSe_2. This result is in agreement with the small SBHs for $\beta_{12}/MoSe_2$ and β_{12}/WSe_2 as compared to β_{12}/MoS_2 and β_{12}/WS_2.

3.3. Effect of In-plane Strains and Vertical Pressure on Schottky Barriers

From Figure 4, it is observed that when the uniaxial ($+a$ and$+b$) strains are applied to β_{12}/MoS_2 heterostructure, the highest occupied states of valence bands (VBs) and lowest unoccupied states of conduction bands (CBs) in MoS_2 shifted (VBMs at Γ shifted from$Y - \Gamma$ and CBMs at $Y - \Gamma$ shown by yellow arrows) towards the Fermi level in such a way that the energy difference between the Fermi level and CBM is less in magnitude as compared to the energy difference between the Fermi level and VBM resulting in tuning of p-type SBHs into n-type and these values are listed in Table 3. Similar observations are obtained for β_{12}/WS_2 under expansion strain ($+b$) but under expansion strain ($+a$) the p-type Schottky contact remains intact (Figure S2 of Supplementary Information (SI)). The biaxial expansions ($+a + b$) at ideal tensile strain

limits for β_{12}/MoS_2 (Figure 4) and β_{12}/WS_2 (Figure S2 of SI) cause the transformation of p-type SBHs into n-type ohmic contact and p-type into n-type SBHs, respectively. In these transformations, the VBMs are shifted from $Y - \Gamma$ to Γ while CBMs are along $Y - \Gamma$ (Table S1 of SI). Moreover, when $\beta_{12}/MoSe_2$ and β_{12}/WSe_2 heterostructures (Figure S1 & S3 of SI) are subjected under the tensile strains (uniaxial$+a$, $+b$ and biaxial$+a+b$), there is a change in SBHs for both electrons and holes (Table 3). However, it is observed that the p-type SBHs are still smaller in magnitude than n-type SBHs, thus these heterostructures with expansion strains have p-type Schottky contacts at the interface. Positions of CBMs and VBMs along high symmetry path have been given in Table S1 of SI. Furthermore, the charge density difference analysis provides an insight into the tuning of p-type Schottky contacts into n-type which is due to the accumulation and depletion of charges at the interface giving rise to the shift in Fermi level.

Next we consider vertical pressure (P) on the heterostructures to see the effect on Schottky Barriers. The pressure has been calculated as, $P = (E - E_0)/(\Delta d)A$; which gives the energy required per unit area to reduce the interlayer distance by $\Delta d = (d_0 - d)$ where E and E_0 are strain-free and strained heterostructures energies of the β_{12}/MX_2 systems, Δd is the change in bilayer distance, A is the area of the unit cell and d_0 and d are the separations in the equilibrium and strained heterostructures, respectively. Variation in the energy magnitudes of VBMs and CBMs with the pressure (Figure 5 (a, c)) suggests that the applied pressure causes the changes in Schottky barriers from p-type to n-type at values of ideal pressures 5.46 GPa and 5.25GPa (at the interlayer distances 2.52 Å & 2.55 Å). Figure 5 (b, d) illustrates that SBHs obtained for holes at the values of ideal pressures 5.0 GPa and 5.13 GPa (interlayer distances of

2.65 Å for both $\beta_{12}/MoSe_2$ and β_{12}/WSe_2) are yet smaller than the SBHs obtained for electrons. Thus, p-type Schottky contacts remain intact at ideal pressure values.

There is observable change in the energy magnitudes of SBHs as compared to the pristine heterostructures, values are tabulated in Table 3. It is observed that VBMs and CBMs are along $Y-\Gamma$ for β_{12}/MX_2 heterostructures (Figure S4 (a-d) of SI) and noticed that the difference in the charge distributions comes from charge distribution of both metal and semiconductor layers at interface that leads to a shift in the SBHs.

Besides the expansion strains, the compression strains are also accountable for tuning of Schottky barriers. Uniaxial compression strain ($-a$ and $-b$) lifts the VBMs of MoS_2 towards the Fermi level. It is noticeable that the VBMs crossing the Fermi level are shifted from $Y-\Gamma$ to Γ and from $Y-\Gamma$ to S high symmetry point for $-a$ and $-b$ strains, respectively, whereas the CBMs remain along $Y-\Gamma$ path. Consequently, the energy magnitude of p-type SBHs gets reduced to zero and that of n-type SBHs gets reduced to the values tabulated in Table 3 suggesting that p-type ohmic contacts are formed at β_{12}/MoS_2 interface. Similarly, p-type ohmic contacts are formed for $\beta_{12}/MoSe_2$, β_{12}/WS_2 and β_{12}/WSe_2 heterostructures (Figures S5-S7 of SI) under $-a$ and $-b$ strains, respectively.

When the β_{12}/MoS_2 (Figure 6) and β_{12}/WS_2 (Figure S6 of SI) heterostructures are subjected under the biaxial compression ($-a-b$) strain, the CBMs of MX_2 shift towards the Fermi level and crosses it along $Y-\Gamma$ path while the VBMs of MoS_2 and WS_2 get shifted from $Y-\Gamma$ to Γ point. It indicates that SBHs for electrons are reduced to zero and have transformed into n-type ohmic contact at β_{12}/MX_2 interface, while the SBHs corresponding to holes are lower than pristine values listed in Table 3. In the same way, biaxial compression ($-a-b$) strains

applied for $\beta_{12}/MoSe_2$ and β_{12}/WSe_2 (Figures S5, S7 and Table S1 of SI) result in the formation of p-type ohmic contact at the interface.

TABLE 3. The Calculated SBHs for electrons **(ϕ_e)** and holes **(ϕ_h)** for unstrained, expansion strained (uniaxial and biaxial), vertical pressure applied and compression strained (uniaxial and biaxial) β_{12}/MX_2 heterostructures.

Types of Strains		System							
		β_{12}/MoS_2 SBHs (eV)		$\beta_{12}/MoSe_2$ SBHs (eV)		β_{12}/WS_2 SBHs (eV)		β_{12}/WSe_2 SBHs (eV)	
		ϕ_e	ϕ_h	ϕ_e	ϕ_h	ϕ_e	ϕ_h	ϕ_e	ϕ_h
Unstrained		**1.04** (1.09)*	**0.64** (0.63)*	**0.96** (1.11)*	**0.32** (0.22)*	**1.25** (1.35)*	**0.53** (0.46)*	**1.15** (1.14)*	**0.20** (0.23)*
Expansion (%)	**+a**	**0.02**	**0.52** @20.0	**0.81**	**0.3** @14.5	**0.29**	**0.33** @20.0	**1.0**	**0.22** @15.0
	+b	**0.58**	**0.65** @12.5	**1.19**	**0.07** @10.5	**0.58**	**0.64** @14.0	**1.34**	**0.17** @10.5
	+a+b	**0**	**0.44** @10.5	**0.52**	**0.39** @10.5	**0.26**	**0.24** @10.5	**0.83**	**0.24** @8.5
Vertical Pressure (GPa)		**0.79**	**1.09** @5.46	**0.79**	**0.67** @5.00	**0.93**	**1.02** @5.25	**1.13**	**0.45** @5.13
Compression (%)	**-a**	**0.55**	**0** @8.8	**0.81**	**0** @2.5	**0.71**	**0** @9.0	**1.04**	**0** @2.5
	-b	**0.71**	**0** @9.0	**0.80**	**0** @3.0	**0.81**	**0** @9.6	**0.89**	**0** @4.0
	-a-b	**0**	**0.29** @10.0	**0.18**	**0** @5.8	**0**	**0.53** @10.0	**0.89**	**0** @5.8

Where * denotes the reported data [50].

In a bid to visualize the charge redistribution at the interface which is accountable for the transitions of SBHs, the charge density difference profiles (Figure 6) provide the quantitative picture under the different compression (uniaxial and biaxial) strains. On applying the uniaxial and biaxial compressive strains to the β_{12}/MX_2 heterostructures ((Figure 6) and (Figures S5-S7 of SI)), electrons transfer from MX_2 to β_{12} pulling down the Fermi level close to the VBM as shown in the band structures, except the case where the biaxial compressive strains induced for

β_{12}/MoS_2 (Figure 6) and β_{12}/WS_2 (Figure S6 of SI) heterostructures result in transfer of electrons from β_{12} to MoS_2 and WS_2 lifting up the Fermi level closer to the CBM.

3.4. Tunneling Characteristics

By and large, the flow of electrical current across the MS interface is non-linear against the applied bias voltage. To see the impact of external uniaxial and biaxial strains applied on the β_{12}/MX_2 heterostructures their tunneling characteristics have been evaluated. In an effort to quantify the change in the electronic properties such as transformation of Schottky contacts into ohmic contacts the $I-V$ characteristics of the heterostructures have been studied using an STM like setup [51]. As per the BTH formalism of electron tunneling, the tunneling current (I) in this model setup [41-43] is given as follows:

$$I = \frac{4\pi e}{\hbar}\int_{-\infty}^{\infty}\rho_s\left(\varepsilon+\frac{eV}{2}\right)\rho_t\left(\varepsilon-\frac{eV}{2}\right)e^{-2d\left(2\left(\frac{m}{\hbar^2}\right)(\varphi_{av}-\varepsilon)\right)^{\frac{1}{2}}}\begin{Bmatrix}\left[f\left(\varepsilon-\frac{eV}{2}\right)\right]\left[1-\left[f\left(\varepsilon+\frac{eV}{2}\right)\right]\right]-\\ \left[f\left(\varepsilon+\frac{eV}{2}\right)\right]\left[1-\left[f\left(\varepsilon-\frac{eV}{2}\right)\right]\right]\end{Bmatrix} \quad (3)$$

where, ρ_t and ρ_s denote the projected density of states (PDOS) of the Au_{13} cluster (tip) and heterostructures (sample), respectively, d symbolizes the distance between the sample and tip, ε represents the injection energy corresponding to the tunneling electrons and f stands for function associated with the Fermi distribution. The average work function (φ_{av}) for both the tip as well as sample and effective electron mass (m) are assumed to be constant corresponding to the applied bias $\pm 1V$. The tip is considered to be separated from the sample by a vacuum barrier 5Å, mimicking a non-bonded tip configuration for the STM measurements [52-54].

Figure 7 (a-b) aims to qualitatively describe the transitions from Schottky contacts to ohmic contacts. To gain an insight into the tunneling characteristics, comparison between the

PDOS of MoS_2 in heterostructures and tip (Au_{13} cluster) has been taken into account as shown in Figure 7(a). In this approach, the tunneling current is given by the convolution of the local density of states of the sample and tip. It is seen from Figure 7 (a) that electrons of the tip or sample do not find the open channels to tunnel; consequently there is no current in the strained β_{12}/MoS_2 heterostructrues at zero bias. In compression $(-a)$ strain, as bias voltage $0.1V$ is applied, the electrons associated with $0.1eV$ (energies) above the Fermi level get the accessible tunnelling channels through the sample, produce tunneling current in small amount. Similarly, on applying compression $(-a-b)$ strain, the electrons find the conduction channels with the increase in bias voltage giving rise to large tunneling current as compared to the current obtained in compression strain $(-a)$. At voltage $+1.0V$, there is decrease in tunneling current because the number of accessible electrons is constant. When bias voltage is $+0.5V$ in case of compression strain $(-b)$, there is less number of conduction channels to tunnel electrons in considered systems resulting in decrease in current. This analysis suggests that the compression strains induced electronic states in the vicinity of Fermi level and these states enable the obtainable conduction channels. As a result the magnitude of tunneling current is increasing.

It has been observed that at very low bias voltage $\pm 0.1V$, all the studied heterostructures under the uniaxial and biaxial compression strain have shown the linear behavior (ohmic behavior) in $I-V$ characteristics as compared to pristine heterostructures which show no tunneling current in the energy region of SBHs. Negative differential resistance (NDR) has also been observed in Figure 7(b) and Figure S8 (a-c) of SI which may be due to less no. of conduction channels for tunneling electrons in the $I-V$ characteristics for positive and negative biases in the compressively strained heterostructures.

4. Conclusions

In summary, on the basis of DFT, we have investigated the strain induced variations in electronic properties and their effect on tunneling characteristics of the β_{12}/MX_2 (M = Mo, W and X = S, Se) vdW heterostructures. It is found that there is no change in the intrinsic electronic nature of both β_{12} and MX_2 upon their contact with each other and the p-type Schottky barriers are formed in pristine β_{12}/MX_2 heterostructures. The in-plane expansion strains such as uniaxial strains cause the transformation of Schottky contacts from p-type to n-type and biaxial strain achieves the formation of n-type ohmic contact at β_{12}/MoS_2 interface. Whereas both the strains (uniaxial and biaxial) applied for β_{12}/WS_2 heterostructure show the transformations from p-type Schottky contact to n-type. While, for $\beta_{12}/MoSe_2$ and β_{12}/WSe_2 there are changes in SBHs but still the contacts are p-type Schottky contacts. Likewise, the electronic properties at the ideal pressure obtained for the MS interface suggest that there is change in SBHs as well as Schottky contact from p-type to n-type for β_{12}/MoS_2 and β_{12}/WS_2 but for $\beta_{12}/MoSe_2$ and β_{12}/WSe_2 change in SBHs has been seen and Schottky contacts are still remain p-type. Further, the in-plane compressive strains (uniaxial and biaxial) at typical values accomplish the transformations from p-type Schottky contact to p-type ohmic in β_{12}/MX_2 heterostructures except the cases, where n-type ohmic contacts are obtained on applying biaxial compressive strain for β_{12}/MoS_2 and β_{12}/WS_2. In selecting a strategy such as the ohmic contacts for some applications, the current carrying ability of the interface is the only quality factor. Therefore, it is found in the tunneling characteristics that at low bias $\pm 0.1V$, the compression strain leads to an ohmic behavior at interface owing to availability of strain-induced conduction channels in the systems. NDR has also been observed which may be due to less no. of conduction channels for tunneling electrons in the $I-V$ characteristics for positive and negative biases in the compressively strained

heterostructures. Our study suggests that the tunability in Schottky barriers with strains can lead to novel β_{12}/MX_2 based nano- and optoelectronic devices.

Acknowledgements

N. Katoch gratefully acknowledges University Grant Commission of India for providing Non-NET fellowship, the CVRAMAN, high performance computing facility at Physics Department, Himachal Pradesh University, Shimla and National Param Supercomputing Facility at CDAC-Pune which have been used to obtain the results presented here.

References

[1] A. K. Geim, K. S. Novoselov, Nat. Mater. , 6 (2007), 183-191.

[2] G. R. Bhimanapati, Z. Lin, V. Meunier, Y. Jung, J. Cha, S. Das, D. Xiao, Y. Son, M. S. Strano, V. R. Cooper, L. Liang, S. G. Louie, E. Ringe, W. Zhou, S. S. Kim, R. R. Naik, B. G. Sumpter, H. Terrones, F. Xia, Y Wang, J. Zhu, D. Akinwande, N. Alem, J. A. Schuller, R. E. Schaak, M. Terrones, J. A. Robinson, ACS Nano, 9 (2015), 11509-11539.

[3] P. Miro, M. Audiffred, T. Heine, Chem. Soc. Rev., 43 (2014), 6537-6554.

[4] X. Kong, Q. C. Liu, C. Zhang, Z. Peng, Q. Chen, Chem. Soc. Rev., 46 (2017), 2127-2157.

[5] A. Ramasubramaniam, D. Naveh, E. Towe, Phys. Rev. B: Condens. Matter Mater. Phys., 84 (2011), 205325.

[6] P. Johri, V. B. Shenoy, ACS Nano, 6 (2012), 5449-5456.

[7] M. Bernardi, M. Palummo, J. C. Grossman, Nano Lett., 13 (2013), 3664-3670.

[8] H. Schmidt, F. Giustiniano, G. Eda, Chem. Soc. Rev., 44 (2015), 7715-7736.

[9] M. Chhowalla, H. Shin, G. Eda, L.-J. Li, K. P. Loh, H. Zhang, Nat. Chem., 5 (2013), 263-275.

[10] A. J. Mannix, X. F. Zhou, B. Kiraly, J. D. Wood, D. Alducin, B. D. Myers, X. Liu, B. L. Fisher, U. Santiago, J. R. Guest, M. J. Yacaman, A. Ponce, A. R. Oganov, M. C. Hersam, N. P. Guisinger, Science, 315 (2015), 1513-1516.

[11] B. Feng, J. Zhang, Q. Zhong, W. Li, S. Li, H. Li, P. Cheng, S. Meng, L. Chen, K. Wu, Nat. Chem., 8 (2016), 563-568.

[12] X. Liu, Z. Wei, I. Balla, A. J. Mannix, N. P. Guisinger, E. Luijten, M. C. Hersam, Sci. Adv., 3 (2017), 1602356.

[13] Z. Zhang, Y. Yang, E. S. Penev, B. I. Yakobson, Adv. Funct. Mater., 27 (2017), 1605059.

[14] L. Adamska, S. Sadasivam, J. J. Foley IV, P. Darancet, S. Sharifzadeh, J. Phys. Chem. C, 122 (2018) 4037-4045.

[15] P. Liang, Y. Cao, B. Tai, L. Zhang, H. Shu, F. Li, D. Chao, X. Du, J. Alloys Compd., 704 (2017), 152-159.

[16] K. S. Novoselov, A. Mishchenko, A. Carvalho, A. H. C. Neto, Science, 353 (2016), aac9439.

[17] B. Liu, L.-J. Wu, Y.-Q. Zhao, L.-Z. Wang, M.-Q. Cai, RSC Adv., 6 (2016), 60271-60276.

[18] Y. Ma, Y. Dai, M. Guo, C. Niu, B. Huang, Nanoscale, 3 (2011), 3883-3887.

[19] P. T. K. Loan, W. Zhang, C.-T. Lin, K.-H. Wei, L.-J. Li, C.-H. Chen, Adv. Mater., 26 (2014), 4838–4844.

[20] W. Zhang, C.-P. Chuu, J.-K. Huang, C.-H. Chen, M.-L. Tsai, Y.-H. Chang, C.-T. Liang, Y.-Z. Chen, Y.-L. Chueh, J.-H. He, M.-Y. Chou, L.-J. Li, Sci. Rep., 4 (2014), 3826.

[21] L. Yu, Y.-H. Lee, X. Ling, E. J. G. Santos, Y. C. Shin, Y. Lin, M. Dubey, E. Kaxiras, J. Kong, H. Wang, T. Palacios, Nano Lett., 14 (2014), 3055-3063.

[22] J. Wang, F. Ma, M.Sun, RSC Adv., 7 (2017), 16801-16822.

[23] G. Li, L. Zhang, W. Xu, J. Pan, S. Song, Y. Zhang, H. Zhou, Y. Wang, L. Bao, Y.-Y. Zhang, S. Du, M. Ouyang, S. T. Pantelides, H.-J. Gao, Adv. Mater., 30 (2018), 1804650.

[24] G. W. Mudd, S. A. Svatek, L. Hague, O. Makarovsky, Z. R. Kudrynskyi, C. J. Mellor, P. H. Beton, L. Eaves, K. S. Novoselov, Z. D. Kovalyuk, E. E. Vdovin, A. J. Marsden, N. R. Wilson, A. Patanè, Adv. Mater., 27 (2015), 3760-3766.

[25] K. Zhang, T. Zhang, G. Cheng, T. Li, S. Wang, W. Wei, X. Zhou, W. Yu, Y. Sun, P. Wang, D. Zhang, C. Zeng, X. Wang, W. Hu, H. J. Fan, G. Shen, X. Chen, X. Duan, K. Chang, N. Dai, ACS Nano, 10 (2016), 3852-3858.

[26] J. E. Padilha, A. Fazzio, A. J. R. d. Silva, Phys. Rev. Lett., 114 (2015), 066803.

[27] S. Kaur, A. Kumar, S. Srivastava, K. Tankeshwar, Phys. Chem. Chem. Phys., 19 (2017), 22023-22032.

[28] A. K. Geim, I. V. Grigorieva, Van der Waals heterostructures, Nature, 499 (2013), 419-425.

[29] D. Jariwala, T. J. Marks, M. C. Hersam, Nat. Mater., 16 (2017), 170-181.

[30] A. J. Mannix, Z. Zhang, N. P. Guisinger, B. I. Yakobson, M. C. Hersam, Nat. Nanotechnol., 13 (2018), 444-450.

[31] R. T. Tung, Appl. Phys. Rev., 1 (2014), 011304.

[32] Y. Jiao, A. Hellman, Y. Fang, S. Gao, M. Kall, Sci. Rep. 5 (2015) 11374.

[33] C. Jin, F. A. Rasmussen, K. S. Thygesen, J. Phys. Chem. C, 119 (2015), 19928-19933.

[34] B. Liu, L.-J. Wu, Y.-Q. Zhao, L.-Z. Wang, M.-Q. Cai, Phys. Chem. Chem. Phys., 18 (2016), 19918-19925.

[35] B. Liu, L.-J. Wu, Y.-Q. Zhao, L.-Z. Wang, M.-Q. Cai, Phys. Chem. Chem. Phys., 17 (2015), 27088-27093.

[36] S. S. Baik, S. Lm, H. J. Choi, Sci. Rep., 7 (2017), 45546.

[37] Xiaoshan Wang, Zhiwei Wang, Jindong Zhang, Xiang Wang, Zhipeng Zhang, Jialiang Wang, Zhaohua Zhu, Zhuoyao Li, Yao Liu, Xuefeng Hu, Junwen Qiu, Guohua Hu, Bo Chen, Ning Wang, Qiyuan He, Junze Chen, Jiaxu Yan, Wei Zhang, Tawfique Hasan, Shaozhou Li, Hai Li, Hua Zhang, Qiang Wang, Xiao Huang, Wei Huang, Nat. Commun., 9 (2018), 3611.

[38] H. V. Phuc, N. N. Hieu, B. D. Hoi, L. T. T. Phuong, C. V. Nguyen, Surf. Sci., 668 (2018), 23-28.

[39] K. He, C. Poole, K. F. Mak, J. Shan, Nano Lett., 13 (2013), 2931-2936.

[40] S. H. Bae, Y. Lee, B. K. Sharma, H.-J. Lee, J.-H. Kim, J.-H. Ahn, Carbon, 51 (2013), 236-242.

[41] J. Bardeen, Phys. Rev. Lett., 6 (1961), 57-59.

[42] J. Tersoff, D. R. Hamann, Phys. Rev. Lett., 50 (1983), 1998-2001.

[43] J. Tersoff, D. R. Hamann, Phys. Rev. B, 31 (1985), 805-813.

[44] G. Kresse, J. Furthmuller, Phys. Rev. B: Condens. Matter Mater. Phys., 54 (1996), 11169-11186.

[45] J. P. Perdew, J. A. Chevary, S. H. Vosko, K. A. Jackson, M. R. Pederson, D. J. Singh, C. Fiolhais, Phys. Rev. B: Condens. Matter Mater. Phys., 46 (1992), 6671-6687.

[46] P. E. Blochl, Phys. Rev. B: Condens. Matter Mater. Phys., 50 (1994), 17953-17979.

[47] L. Shulenburger, A. D. Baczewski, Z. Zhu, J. Guan, D. Tomanek, Nano. Lett., 15 (2015), 8170-8175.

[48] A. Kumar, P. K. Ahluwalia, Modell. Simul. Mater. Sci. Eng., 21 (2013), 065015.

[49] F. Zhang, W. Li, Y. Ma, Y. Tang, X. Dai, RSC Adv., 7 (2017), 29350-29356.

[50] J. Yang, R. Quhe, S. Feng, Q. Zhang, M. Lei, J. Lu, Phys. Chem. Chem. Phys., 19 (2017), 23982-23989.

[51] S. K. Gupta, H. He, D. Banyai, A. K. Kandalam, R. Pandey, J. Chem. Phys., 139 (2013), 244307.

[52] A. Kumar, D. Banyai, P. K. Ahluwalia, R. Pandey, S. P. Karna, Phys. Chem. Chem. Phys., 16 (2014), 20157-20163.

[53] S. Nigam, S. Gupta, D. Banyai, R. Pandey, C. Majumder, Phys. Chem. Chem. Phys., 17 (2015), 6705-6712.

[54] P. Jamdagni, A. Kumar, A. Thakur, R. Pandey, P. K. Ahluwalia, J. Phys. Condens. Matter, 29 (2017), 395501.

Figures of Manuscript

Strain Tunable Schottky Barriers and Tunneling Characteristics of Borophene/MX_2 van der Waals Heterostructures

Neha Katoch[1*], Ashok Kumar[2], Raman Sharma[3], P.K. Ahluwalia[3] and Jagdish Kumar[1]

[1]*Department of Physics and Astronomical Science, School of Physical and Material Sciences, Central University of Himachal Pradesh, Dharamshala, 176215 (India)*

[2]*Department of Physical Science, School of Basic and Applied Sciences, Central University of Punjab, Bathinda, 151001(India)*

[3]*Department of Physics, Himachal Pradesh University, Shimla, 171005 (India)*

[*]Email:
Neha Katoch (nehakatoch2@gmail.com)

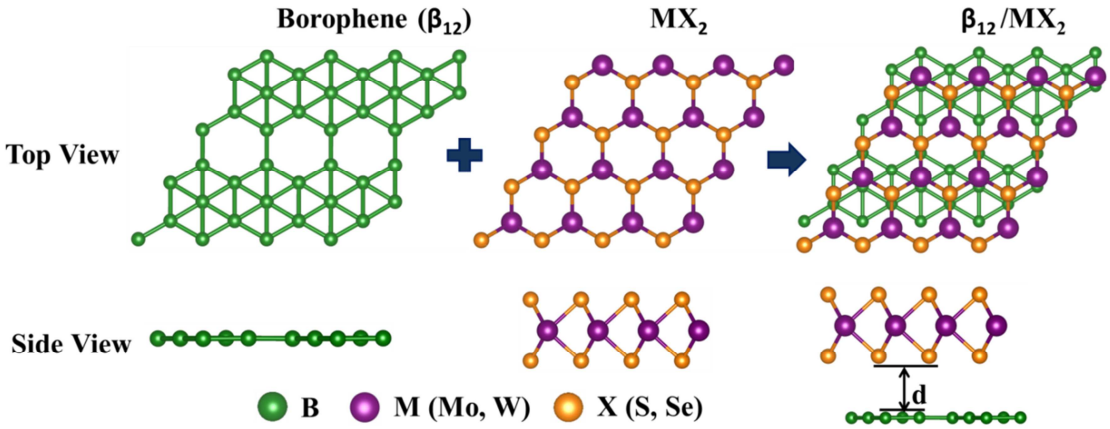

Figure 1. Ball and stick model with respective top and side views of pristine β_{12}, MX_2 and their heterostructures β_{12}/MX_2.

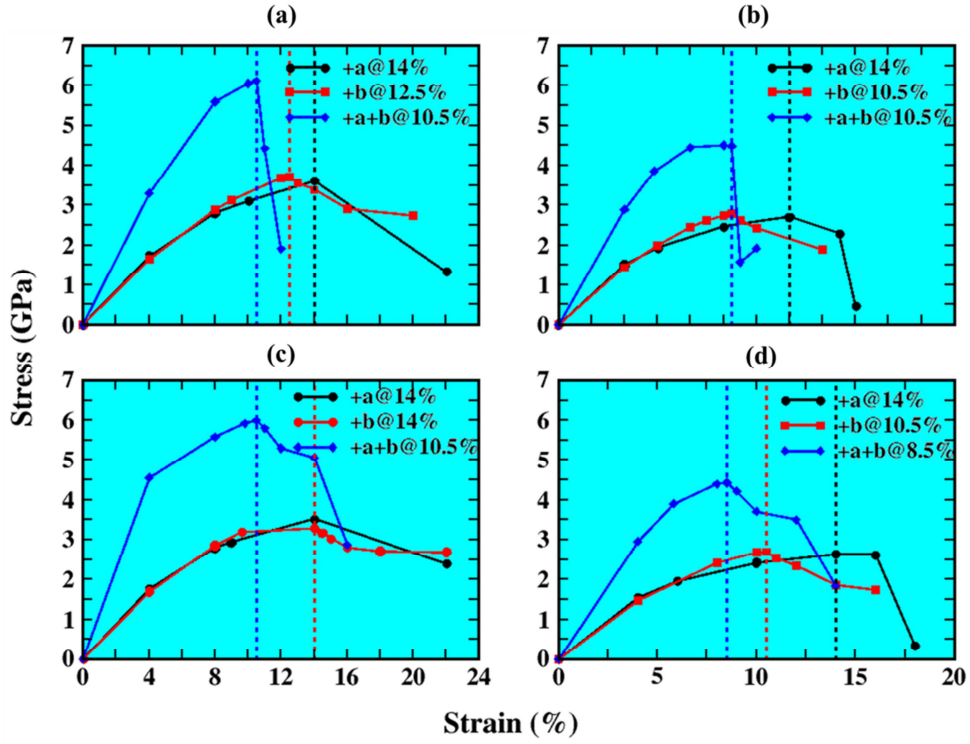

Figure 2. The strain-stress curves for the in-plane expansion strains (uniaxial and biaxial) applied to **(a)** β_{12}/MoS_2, **(b)** $\beta_{12}/MoSe_2$, **(c)** β_{12}/WS_2 and **(d)** β_{12}/WSe_2 heterostructures respectively. Black, red and blue dotted lines denote the tensile strain limits for $+a$, $+b$ and $+a+b$ respectively.

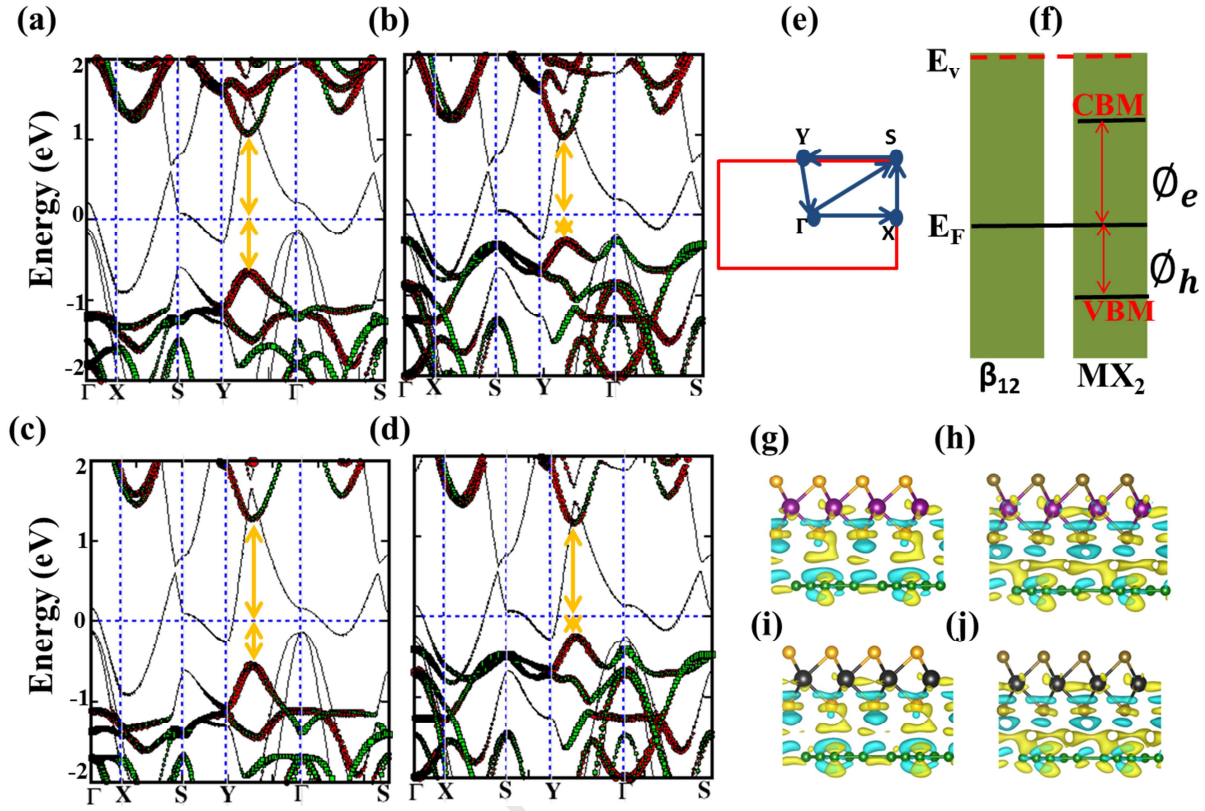

Figure 3. OPBS for pristine **(a)** β_{12}/MoS_2, **(b)** $\beta_{12}/MoSe_2$, **(c)** β_{12}/WS_2 and **(d)** β_{12}/WSe_2, heterostructures, respectively. Black lines are for β_{12}, whereas width of the bands shows the weight factor where red and green lines denote the contribution from Mo-d (W-d) and S-p (Se-p) orbitals of atoms. The dashed line at 0 eV represents the Fermi level and yellow arrow indicates the transition from VBM to CBM. **(e)** Represents the brillouin zone of the heterostructures with high symmetry path **(f)** A schematic of the β_{12}/MX_2 interface Schottky contact. The n-type ($\emptyset_e$) and p-type ($\emptyset_h$) SBHs are indicated by the difference between the CBM and VBM of MX_2 and the Fermi level, respectively. Charge density difference profiles **(g-j)** for heterostructures in accordance to **(a-d)** have been shown. Isosurface value is set at 2.4×10^{-4} e/Å^3 where yellow region shows charge accumulation while blue region is for charge depletion.

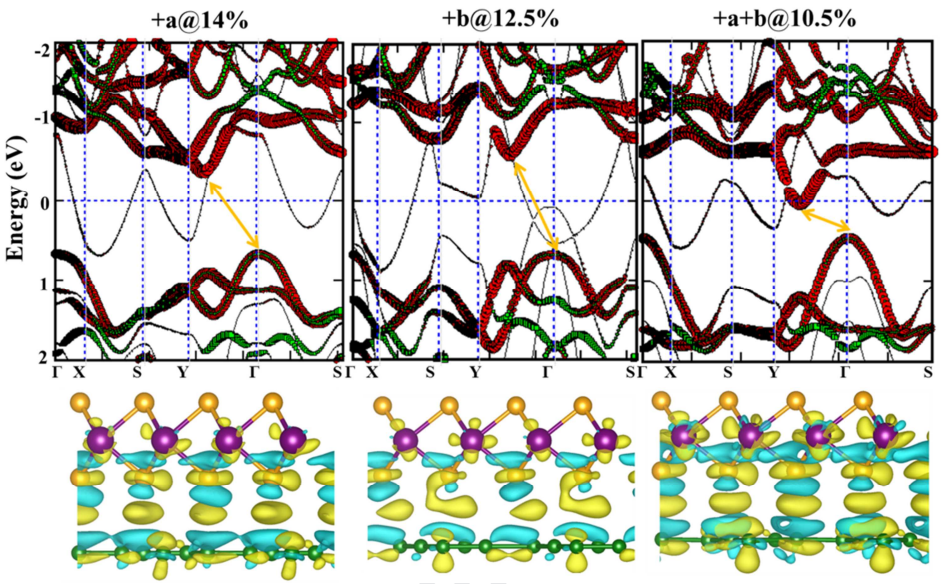

Figure 4. OPBS for tensile strains, uniaxial ($+a$ and$+b$) and biaxial ($+a+b$) applied to β_{12}/MoS_2 heterostructure. Black lines are for β_{12}, whereas width of the bands shows the weight factor where red and green lines denote the contribution from Mo-d and S-p orbitals of atoms. The Fermi level is at 0 eV, represented by dashed line and yellow arrow indicates the transition. Charge density difference profiles for heterostructure at different values of strains have been shown below the band structures. Isosurface value is set at 2.4×10^{-4} e/Å^3 where yellow region shows charge accumulation while blue region is for charge depletion.

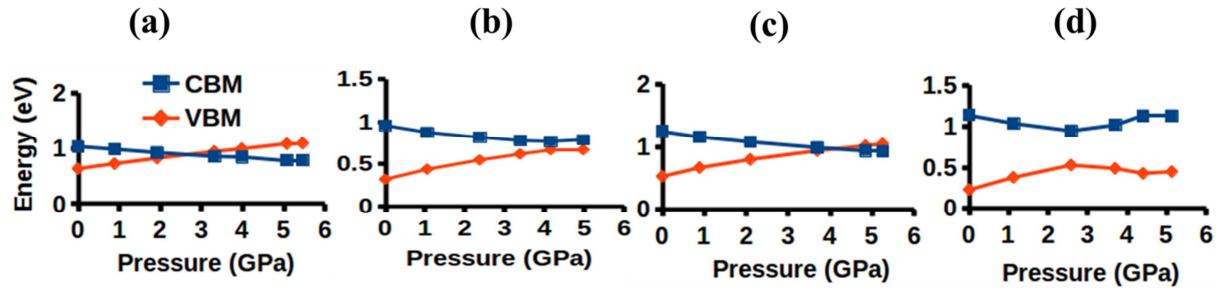

Figure 5. Variation in the energy magnitudes of CBM and VBM with pressure applied on **(a)** β_{12}/MoS_2, **(b)** $\beta_{12}/MoSe_2$, **(c)** β_{12}/WS_2 and **(d)** β_{12}/WSe_2 heterostructures respectively.

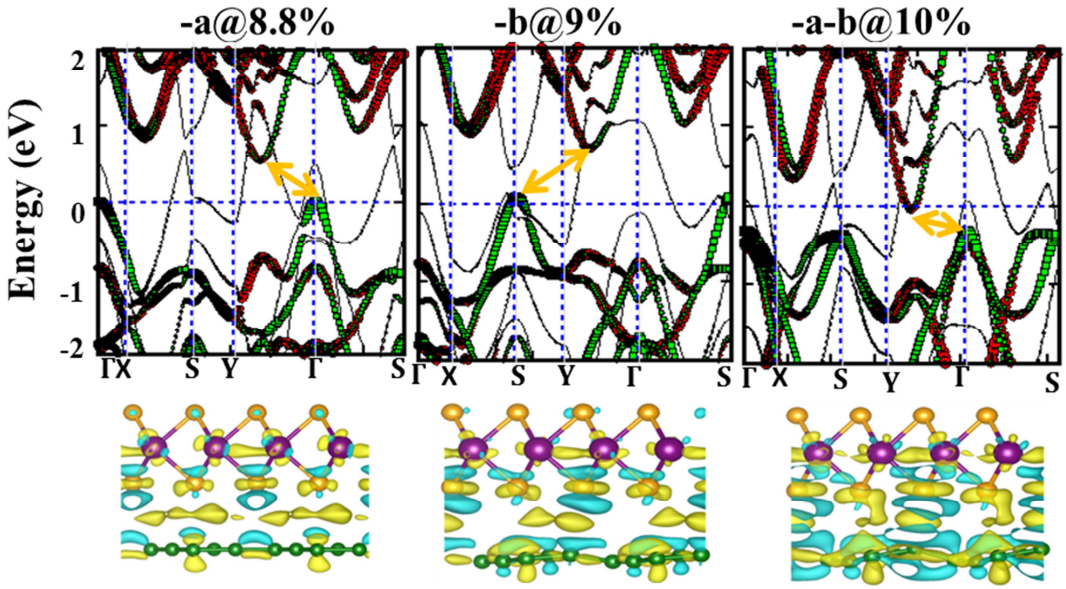

Figure 6. OPBS for in-plane compression uniaxial ($-a$ and$-b$) and biaxial ($-a-b$) strains applied to β_{12}/MoS_2 heterostructure. Black lines are for β_{12}, whereas width of the bands shows the weight factor where red and green lines denote the contribution from Mo-d and S-p orbitals of atoms. Yellow arrows and dashed line indicate the transitions from VBM to CBM and Fermi level (at 0 eV), respectively. The associated charge density difference profiles for heterostructures at different strain values have been shown below the band structures. Isosurface value is set at 2.4×10^{-4} e/Å^3 where yellow region shows charge accumulation while blue region is for charge depletion.

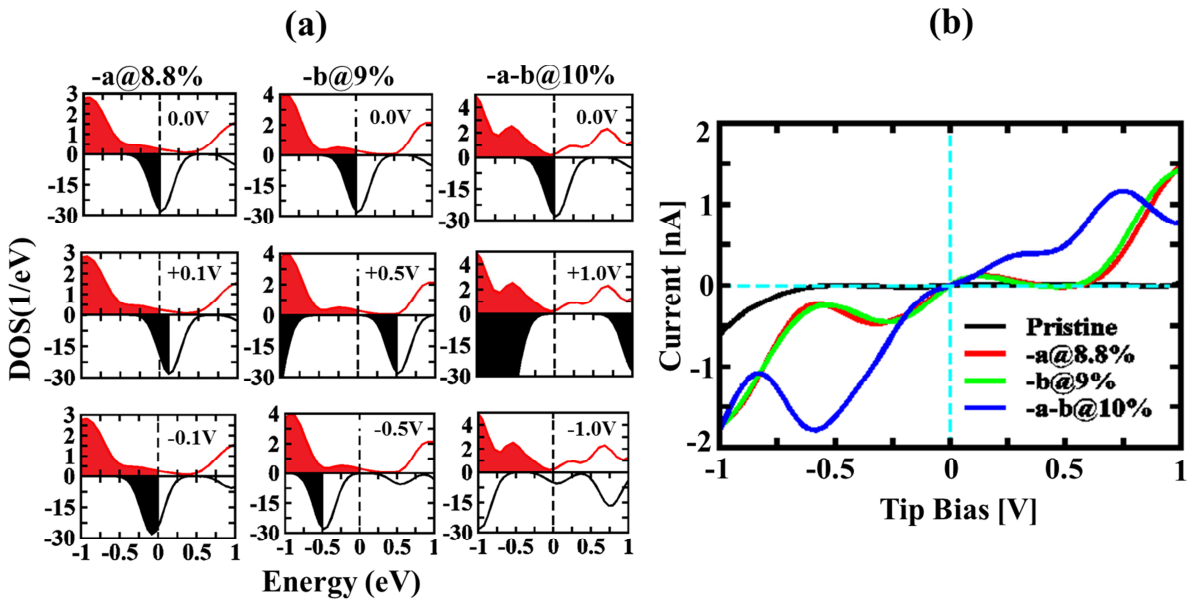

Figure 7. (a) Depiction of the density of states (DOS) of β_{12}/MoS_2 sample (in positive y-axis) of with compression strains; $-a$, $-b$ and $-a-b$ and Au_{13} tip (in negative y- axis), at different applied bias voltage where black and red shaded regions represent the occupied states of sample and tip respectively. **(b)** The $I-V$ characteristics of pristine and the compressive strains (uniaxial and biaxial) induced β_{12}/MoS_2 heterostructure.

Highlights

- Application of external strains results in a considerable transformation of Schottky barriers from p-type to n-type and to ohmic contacts.
- The applied compressive strains lead to ohmic behavior at low bias $\pm 0.1\ V$.
- $I-V$ characteristics exhibit noticeable Negative differential resistance (NDR) for compressively strained heterostructures.

Author declaration

It is stated that no conflicts of interest exist associated with this manuscript entitled “Strain Tunable Schottky Barriers and Tunneling Characteristics of Borophene/MX_2 van der Waals Heterostructures". The manuscript has been read and approved by all named authors and they have also given their consent to send this paper to the journal *Physica E: Low-dimensional Systems and Nanostructures*.

Corresponding Author

Neha Katoch